Urban Climate 65 (2026) 102795

Contents lists available at ScienceDirect

Urban Climate

journal homepage: www.elsevier.com/locate/uclim

# A simplified method to calculate atmospheric $CO_2$ equivalency for changing surface albedo☆

Hashem Akbari *

*Heat Island Group, Concordia University, Montreal, Canada*

ARTICLE INFO

*Keywords:*
High albedo surfaces
$CO_2$ offset
Urban Heat Island
Global warming adaptation

ABSTRACT

Urban surfaces (roofs, pavements) with high solar reflectance (albedo), defined as cool surfaces, reduce solar energy absorbed by buildings and pavements, leading to a reduction in air-conditioning use and improved indoor thermal condition in non-conditioned buildings. In addition, cool surfaces improve summertime outdoor environment that in turn yield a better urban air quality, reduce morbidity and mortality. A reduction in cooling energy use reduces demand for electricity generation and lowers $CO_2$ emissions from fossil fuel power plants. Independent of the direct $CO_2$ reduction, high-albedo urban surfaces reflect a greater fraction of solar shortwave radiation back to space and create a negative radiative forcing (RF) that counters the RF induced by accumulation of greenhouse gases (primarily $CO_2$) in the atmosphere. Previously, a method based on equating the RF on top of the atmosphere (TOA) was introduced to calculate a *global-averaged* $CO_2$ equivalency offset for increasing albedo of urban surfaces. Here, a simplified technique is introduced to calculate a *regional* $CO_2$-equivalency of changes on albedo of land surfaces. The required input for this technique is the regional global horizontal insolation (GHI) on TOA and on ground surface. Using this simplified model, calculations are carried out for about 4400 weather stations world-wide. These calculations showed that the world-wide median $CO_2$ offset was about 2 kg per 0.01 albedo change of a m$^2$ of a surface. The $CO_2$ offset is highest where the atmospheric transmittance is high. The $CO_2$ offset is about 2–3 kg around the equator, 1.5–4 kg for −30° to −20° latitude and 1–5 kg for 20° to 30° latitude, depending on local cloud cover. This method would allow development of country-specific policies to monetize the effect of high-albedo urban surfaces to counter global warming and climate change.

## 1. Introduction

Urban surfaces (roofs and pavements) with high solar reflectance (hereafter referred as cool surfaces) absorb less of incoming shortwave solar radiation and stay cooler under the sun. A cool roof conducts less heat into the building resulting in less air-conditioning energy use in conditioned buildings and improves comfort in non-conditioned buildings (Akbari et al., 1999). In some commercial buildings, application of a cool roof may result in downsizing of the air conditioner and air handler systems that run more efficiently during the partial-load conditions and even save electricity during heating season by using less electricity for air-handling

☆ An earlier draft of this paper with limited results was presented at the 6th International Conference on Countermeasures to Urban Heat Island, Melbourne, Australia, December 4–7, 2023. This paper has modified the methodology and provides detail results for over 200 countries

* Corresponding author.
*E-mail address:* Hashem.Akbari@Concordia.ca.

https://doi.org/10.1016/j.uclim.2026.102795
Received 17 July 2025; Received in revised form 11 December 2025; Accepted 16 January 2026
Available online 6 February 2026

systems (Hosseini and Akbari, 2016).

Cool roofs and cool pavements (together an independently) alter the surface heat balance at a community level which can result in a lower summer time ambient temperature and reduce urban heat island. Lower summertime ambient temperatures typically result in a better ambient air quality (lower concentration of pollutants), improved pedestrian comfort, and lower morbidity and mortality during heat storms (Jandaghian and Akbari, 2021).

Cool roofs and pavements also reflect a significant fraction of incoming shortwave solar radiation that escape the Earth's atmosphere helping to counter global warming. This aspect of reflective surfaces is referred to as a geoengineering technology. Scientists have been studying geoengineering technologies as methods to rapidly respond to extreme climate change (Vaughan and Lenton, 2011). These technologies, naming a few, include: increasing reflectance of large surfaces on the earth, increasing the atmospheric reflectance by injecting reflective particles in the atmosphere, and sequestering $CO_2$ from the atmosphere.

Increasing reflectance of the atmosphere and large land areas are experiments that their consequences are not fully understood. In contrast, humans have a long history of living in areas with white buildings and white cities throughout many parts of the world—cool cities.

Reducing atmospheric $CO_2$ concentration and increasing earth's albedo both cause a negative radiative forcing (RF) that result in slowing the rate of global warming. By equating the RF of incremental $CO_2$ emissions and increasing surface albedo, Akbari et al. (2009) conducted a study to calculate a *global* equivalency between increasing reflectance of urban surfaces and reducing $CO_2$ emissions. They reported that increasing albedo of 1 $m^2$ of a surface by 0.01 has the same effect on slowing the global warming as reducing $CO_2$ emission by about 2.5 kg. Akbari et al. (2012) further expanded this analysis by conducting simulations of the changes in the earth atmosphere temperature by increasing surface albedo and $CO_2$ emissions abatement. They reported that increasing the albedo of 1$m^2$ of a surface by 0.01 would have the same effect on long-term atmospheric temperature as reducing $CO_2$ emissions by 7 kg. The Intergovernmental Panel for Climate Change (IPCC) in their 5th assessment report adopted this 7 kg $CO_2$ offset for increasing surface albedo (IPCC, 2014). Both studies reported only the world-wide effects; regional effects were not evaluated.

The RF from increasing surface albedo is expected to be most effective in regions with high insolation and less clouds. Here, we develop a method to calculate the incoming solar radiation on top of the atmosphere (TOA) for a given location. Then using locally available global horizontal insolation (GHI), we calculate the local atmospheric transmittance and top of the atmosphere RF by increasing a surface albedo. We equate this RF of albedo change with RF from $CO_2$ emissions to develop a *regional* equivalency between surface albedo change and global $CO_2$ emission reduction. We carry out calculations for about 4400 stations around the world. The results are grouped together and presented by countries. The method can be used to develop a $CO_2$ equivalency (offset) and surface albedo change for a given location.

## 2. Methodology

To estimate the $CO_2$ offset by increasing surface albedo, we use a net zero energy balance of Radiative Forcing (RF) on top of the atmosphere (TOA),

$$dRF_{albedo} + dRF_{CO2} = 0 \tag{1}$$

The albedo RF is estimated by

$$dRF_{albedo} = I\, da_{surface}\, f/A \tag{2}$$

Where, $dRF_{albedo}$ = TOA change in RF, $Wm^{-2}$; $I$ = Global Horizontal Insolation (direct and diffuse), $Wm^{-2}$; $da_{surface}$ = Change in albedo for a $m^2$ of a surface; $f$ = Atmospheric transmission of reflected solar radiation; $A$ = Earth surface area, $510.1 \times 10^{12}$ $m^2$.

For $CO_2$ RF, we use Myhre et al. (1998) equation

$$RF_{CO2} = 5.35 \ln(C/C_0) \tag{3}$$

Where, $RF_{CO2}$ = $CO_2$ induced RF, $Wm^{-2}$; $C$ = Atmospheric $CO_2$ concentration; $C_0$ = Reference atmospheric $CO_2$ concentration. In these calculations, the $CO_2$ concentration is assumed to be globally uniform.[1]

The incremental change in RF is calculated by

$$dRF_{CO2} = 5.35\, dC/C \tag{4}$$

Substituting (2) and (4) in (1),

[1] "Atmospheric CO2 concentrations fluctuate slightly with the seasons, falling during the Northern Hemisphere spring and summer as plants consume the gas and rising during northern autumn and winter as plants go dormant or die and decay. The level drops by about 6 or 7 ppm (about 50 Gt) from May to September during the Northern Hemisphere's growing season, and then goes up by about 8 or 9 ppm. The Northern Hemisphere dominates the annual cycle of CO2 concentration because it has much greater land area and plant biomass in mid-latitudes (30–60 degrees) than the Southern Hemisphere. Concentrations reach a peak in May as the Northern Hemisphere spring greenup begins, and decline to a minimum in October, near the end of the growing season. [1][2]Concentrations also vary on a regional basis, most strongly near the ground with much smaller variations aloft. In urban areas concentrations are generally higher [3] and indoors they can reach 10 times background levels." Wikipedia 2025; retrieved 8 December 2025 that include: Rasmussen, 2023; CDIAC. 2007; George et al., 2007.

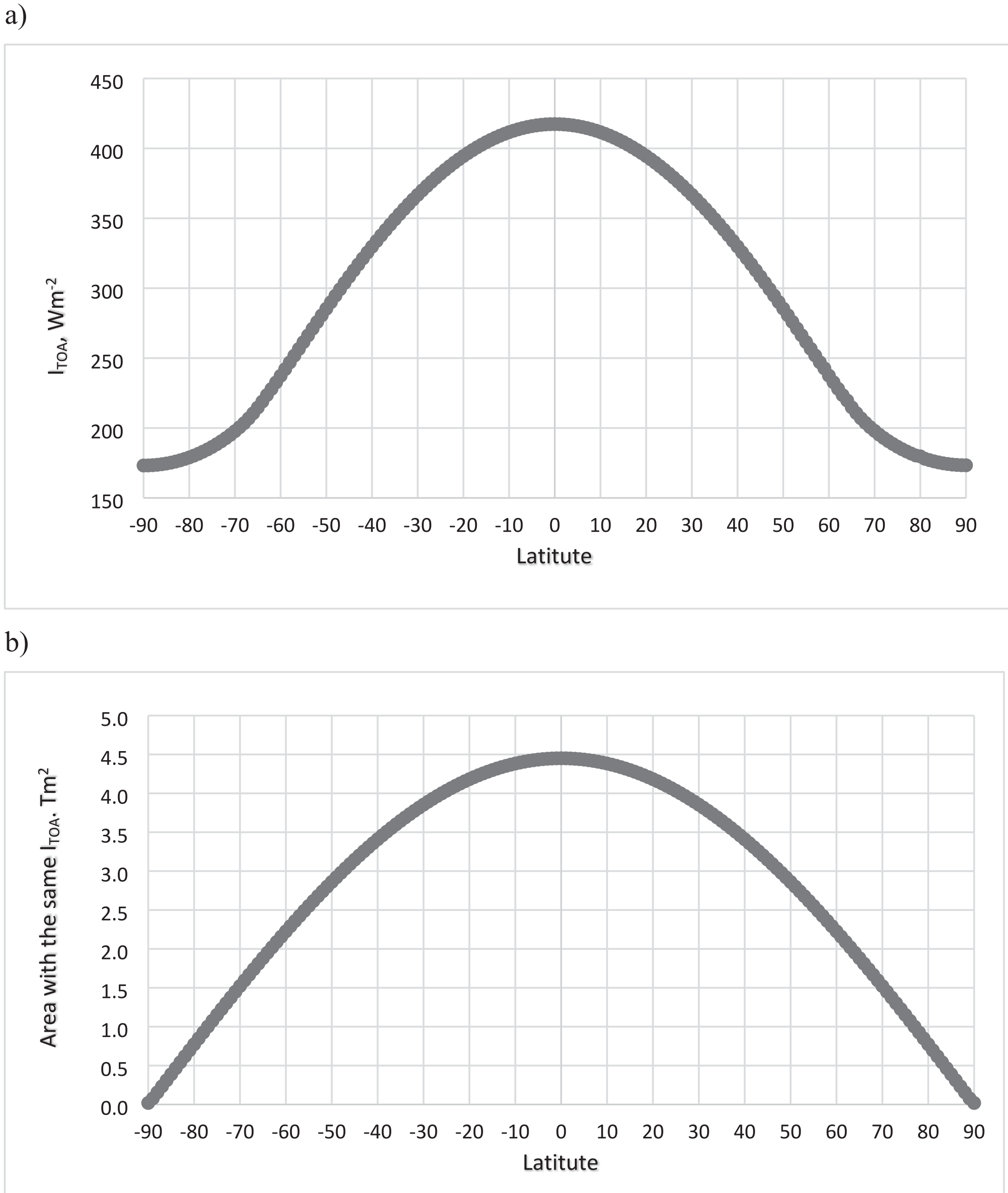


**Fig. 1.** Calculated a) average annual horizontal TOA insolation and b) area of the Earth for a given latitude $\pm 0.5^{\circ}$, $Tm^2$ ($10^{12}$ $m^2$).

$$I\,f\frac{da_{surface}}{A} + 5.35\frac{dC}{C} = 0 \tag{5}$$

Or,

$$dC/da_{surface} = -fIC/5.35A \tag{6}$$

The atmospheric $CO_2$ concentration in 2022 was 421 ppm (NOAA, 2022). Each ppm of atmospheric $CO_2$ concentration is about $7.821 \times 10^{12}$ kg of $CO_2$. Hence, the total atmospheric $CO_2$ content is about $3.293 \times 10^{15}$ kg. Substituting the values of C and A, we get.

$$dC/da_{surface} = -1.21\,f\,I, \text{kg/unit change of a m}^2 \text{ of surface albedo} \tag{7}$$

This equivalency can be represented per 0.01 change in the surface albedo as.

$$dC/da_{surface} = -1.21x10^{-2}f\,I, \quad \text{kg/0.01 change of a m}^2 \text{ of surface albedo} \tag{8}$$

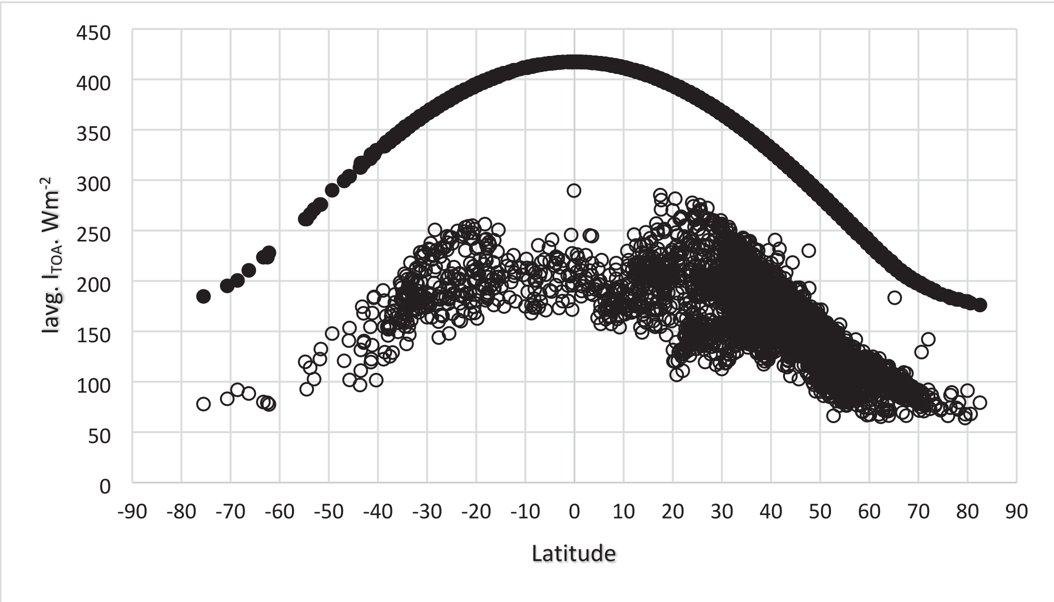


**Fig. 2.** Top of Atmosphere and surface Global Horizontal Insolation, $Wm^{-2}$.

Eq. 8 can be used on an hourly, daily, monthly and yearly basis to estimate the $CO_2$ offset for change in surface albedo. The total horizontal solar radiation, *I*, is a function of the time of the day, day of the year and seasonal climate conditions. Hence, the calculated hourly $CO_2$ equivalency ($CO_2$ offset) can vary significantly throughout hours of the year. A more stable $CO_2$ offset can be calculated by using the hourly values averaged for the year, i.e.

$$\left(dC/da_{surface}\right)_{annual\ avg} = -1.21x10^{-2} I_{annual\ avg} f_{annual\ avg} \tag{9}$$

Assuming the outgoing atmospheric transmission *f* is the same as incoming transmission, the atmospheric solar scattering and attenuation can be calculated by dividing *I* to the calculated TOA incoming solar radiation intensity ($I_{TOA}$),

$$f_{annual\ avg} = \frac{I_{annual\ avg}}{I_{TOA,annual\ avg}} \tag{10}$$

Then Eq. 9 is revised to

$$\left(dC/da_{surface}\right)_{annual\ avg} = -1.21x10^{-2} I^2_{annual\ avg} \Big/ I_{TOA,annual\ avg} \tag{11}$$

It is estimated that *dC* (change in $CO_2$ atmospheric concentration) is only a fraction *g* (~0.5) of the emitted $CO_2$, $C_{emitted}$. Hence, Eq. 11 is scaled to show the emitted-$CO_2$ offset

$$\left(dC_{emitted}/da_{surface}\right)_{annual\ avg} = \frac{-1.21x10^{-2}}{g} I^2_{annual\ avg} \Big/ I_{TOA,annual\ avg} \tag{12}$$

And with g = 0.5,

$$\left(dC_{emitted}/da_{surface}\right)_{annual\ avg} = -2.42x10^{-2} I^2_{annual\ avg} \Big/ I_{TOA,annual\ avg} \tag{13}$$

The extraterrestrial solar radiation on a horizontal surface for a given hour *i* of the day. $I_{TOA,i}$, is calculated by Eq. 14

$$I_{TOA,i} = I_0 \left(1 + 0.033 \cos\left(\frac{360n}{365}\right)\right) (\cos\varphi \cos\delta \cos\omega + \sin\varphi \sin\delta) \tag{14}$$

Where, $I_0$ = Solar constant, 1367 $Wm^{-2}$; $n$ = Day number, Jan 1 = 1; $\varphi$ = Latitude; $\delta$ = Declination angle, and; $\omega$ = Hour angle, 0 at solar noon. The $I_{TOA,\ annual\ avg}$ is calculated by averaging Eq. 14 over 8760 h.

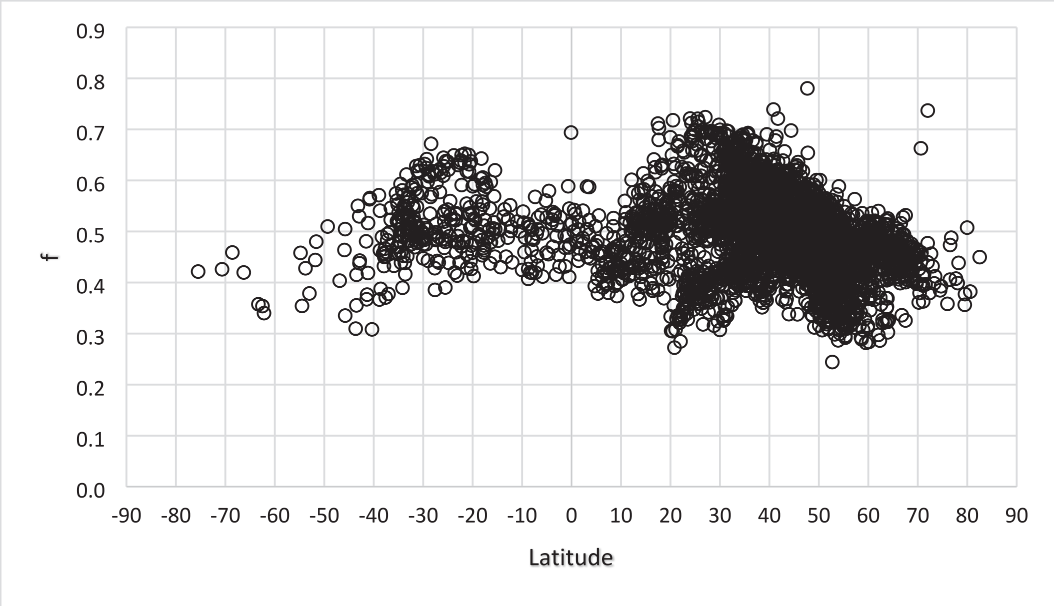


**Fig. 3.** Annual average atmospheric solar transmittance $f_{annual\ avg}$. Note that $f_{annual\ avg}$ is around 0.5 around equator and it typically increases to a range of 0.65–0.75 around latitude ±30°.

**Table 1**
Annual average solar energy transmittance through the atmosphere.

| | Minimum | 1st Quartile | Median | 3rd quartile | Maximum |
|---|---|---|---|---|---|
| All locations | 0.25 | 0.44 | 0.48 | 0.54 | 0.79 |
| Northern Hemisphere | 0.25 | 0.44 | 0.48 | 0.54 | 0.79 |
| Southern Hemisphere | 0.31 | 0.46 | 0.50 | 0.55 | 0.69 |

In Eq. 13, measured hourly, daily, and annual values of $I$ is usually available for many weather stations around the globe (ASHRAE, 2012; NREL, 2008; Merket, 2020).

We calculate the annual average TOA extraterrestrial solar intensity on a horizontal surface, $I_{TOA}$, for each latitude $\varphi$ (location of a city or weather station) by calculating the average of $I_{TOA,i}$ over 24 h of the day and over all declination angles. In our calculations, the global horizontal Insolation were extracted from weather data that included: station name, station WMO number, latitude, longitude, elevation, annual global horizontal insolation in kWh/m$^2$, and direct normal insolation in kWh/m$^2$. The annual insolation was calculated from these three "typical year" data sets: for the U.S., NREL (2008); for Canada, White Box Technologies (2014); and for all other international locations, ASHRAE (2012). Typical year weather data are generated from actual annual data and represents the long-term (about 20 years) average weather conditions.

## 3. Procedure

1. We first calculated monthly averaged $I_{TOA}$, followed by annual averaged, for all latitude at one-degree interval form −90° to +90° and created a summary table. We checked our calculations by computing the average annual incoming solar radiation (weighted by degree latitude area) and comparing it with 1367/4 = 341.8 Wm$^{-2}$. The calculations were exact. Fig. 1a shows the calculated $I_{TOA}$ for all latitudes. Fig. 1b shows the calculated area of the earth for each latitude angle with ±0.5°. The average insolation on the earth was calculated by integrating values in Fig. 1a as weighted by earth area with the same $I_{TOA}$ (Fig. 1b) resulting in 341.8 Wm$^{-2}$.

**Table 2**
Earth shortwave energy balance.

| | Cloud and atmospheric reflectance | Atmospheric absorptance | Atmospheric transmittance | Surface reflectance |
|---|---|---|---|---|
| Kiehl and Trenberth, 1997 | 0.225 | 0.195 | 0.58 | 0.09 |
| NASA | 0.225 | 0.225 | 0.55 | 0.07 |
| Loeb et al., 2021 | 0.226 | 0.227 | 0.547 | 0.087 |
| This study, median | | | 0.485 | |

**Table 3**
$CO_2$ offset (kg) by increasing albedo of a $m^2$ of a surface by 0.01. The $CO_2$ offset is the highest in countries with minimal cloud cover, typically around 20° to 30° latitude. The world median offset is about 1.8 kg.

| Country | Minimum | 1st Quartile | Median | 3rd Quartile | Maximum |
|---|---|---|---|---|---|
| Antigua and Barbuda | 2.8 | 2.8 | 2.8 | 2.8 | 2.8 |
| United Arab Emirates | 4.0 | 4.0 | 4.1 | 4.3 | 4.4 |
| Argentina | 1.2 | 2.0 | 2.2 | 2.4 | 3.5 |
| Armenia | 2.5 | 2.5 | 2.5 | 2.5 | 2.5 |
| American Samoa | 1.8 | 1.8 | 1.8 | 1.8 | 1.8 |
| Antarctica | 0.6 | 0.7 | 0.8 | 0.9 | 1.0 |
| Australia | 0.7 | 2.0 | 2.6 | 3.4 | 4.0 |
| Austria | 1.2 | 1.4 | 1.6 | 1.9 | 2.2 |
| Azerbaijan | 1.9 | 2.0 | 2.0 | 2.0 | 2.1 |
| Belgium | 0.9 | 1.0 | 1.1 | 1.1 | 1.3 |
| Benin | 1.5 | 1.7 | 1.8 | 2.0 | 2.1 |
| Burkina Faso | 2.3 | 2.3 | 2.3 | 2.3 | 2.4 |
| Bulgaria | 1.7 | 1.8 | 1.9 | 2.1 | 2.8 |
| Bahrain | 2.3 | 2.3 | 2.3 | 2.3 | 2.3 |
| Bahamas | 2.5 | 2.5 | 2.5 | 2.5 | 2.5 |
| Bosnia and Herzegovina | 1.6 | 1.6 | 1.7 | 1.9 | 2.2 |
| Belarus | 1.2 | 1.4 | 1.4 | 1.5 | 1.6 |
| Belize | 1.8 | 1.8 | 1.8 | 1.8 | 1.8 |
| Bolivia | 2.1 | 2.1 | 2.5 | 3.0 | 3.4 |
| Brazil | 1.4 | 1.9 | 2.2 | 2.5 | 2.9 |
| Barbados | 2.1 | 2.1 | 2.1 | 2.1 | 2.1 |
| Brunei | 2.2 | 2.2 | 2.2 | 2.2 | 2.2 |
| Botswana | 2.9 | 2.9 | 2.9 | 3.1 | 3.3 |
| Cocos Island | 2.1 | 2.6 | 2.6 | 2.6 | 2.6 |
| Switzerland | 1.1 | 1.4 | 1.6 | 2.1 | 2.5 |
| Chile | 0.9 | 1.6 | 2.1 | 2.7 | 3.2 |
| China | 0.8 | 1.5 | 2.0 | 2.4 | 3.9 |
| Cote D'ivoire | 1.7 | 1.7 | 1.7 | 1.7 | 1.7 |
| Cook Islands | 2.0 | 2.0 | 2.0 | 2.0 | 2.0 |
| Colombia | 1.6 | 1.7 | 2.4 | 2.7 | 3.5 |
| Cabo Verde | 2.7 | 2.7 | 2.7 | 2.7 | 2.7 |
| Costa Rica | 2.1 | 2.1 | 2.1 | 2.1 | 2.1 |
| Cuba | 2.5 | 2.5 | 2.5 | 2.5 | 2.5 |
| Cyprus | 2.5 | 2.5 | 2.5 | 2.6 | 2.6 |
| Czechia | 1.1 | 1.2 | 1.3 | 1.4 | 2.3 |
| Germany | 0.8 | 1.0 | 1.1 | 1.2 | 1.7 |
| Denmark | 0.6 | 0.8 | 1.0 | 1.0 | 1.1 |
| Dominican Republic | 2.5 | 2.5 | 2.6 | 2.6 | 2.7 |
| Algeria | 2.2 | 2.6 | 2.9 | 3.9 | 4.4 |
| Egypt | 3.1 | 3.6 | 4.2 | 4.5 | 4.8 |
| Western Sahara | 3.5 | 3.5 | 3.5 | 3.5 | 3.5 |
| Spain | 1.0 | 2.0 | 2.3 | 2.6 | 3.0 |
| Estonia | 1.2 | 1.3 | 1.3 | 1.3 | 1.3 |
| Finland | 1.0 | 1.1 | 1.2 | 1.3 | 1.5 |
| Fiji | 2.0 | 2.0 | 2.0 | 2.0 | 2.0 |
| Falkland Island | 1.3 | 1.3 | 1.3 | 1.3 | 1.3 |
| France | 0.8 | 1.1 | 1.3 | 1.7 | 3.1 |
| Faroe Island | 0.5 | 0.5 | 0.5 | 0.5 | 0.5 |
| Micronesia | 1.4 | 1.4 | 1.5 | 1.6 | 1.8 |
| Great Britain | 0.5 | 0.7 | 0.8 | 1.0 | 1.2 |
| Georgia | 2.0 | 2.0 | 2.0 | 2.0 | 2.0 |
| Guernsey | 0.8 | 0.8 | 0.8 | 0.8 | 0.8 |
| Gibraltar | 2.2 | 2.2 | 2.2 | 2.2 | 2.2 |
| Greece | 2.1 | 2.3 | 2.3 | 2.4 | 2.6 |
| Grenada | 2.5 | 2.5 | 2.5 | 2.5 | 2.5 |
| Greenland | 1.0 | 1.1 | 1.1 | 1.4 | 1.4 |
| French Guiana | 2.6 | 2.6 | 2.6 | 2.6 | 2.6 |
| Guam | 1.8 | 2.0 | 2.1 | 2.3 | 2.4 |
| Honduras | 1.8 | 1.9 | 2.0 | 2.3 | 2.5 |
| Hungary | 1.3 | 1.5 | 1.5 | 1.6 | 1.9 |
| Indonesia | 1.7 | 2.1 | 2.5 | 2.7 | 3.5 |
| Isle of Man | 0.7 | 0.7 | 0.7 | 0.7 | 0.7 |
| India | 1.6 | 2.5 | 2.8 | 3.1 | 3.7 |
| British Indian Ocean | 1.8 | 1.8 | 1.8 | 1.8 | 1.8 |
| Ireland | 0.6 | 0.7 | 0.7 | 0.7 | 0.8 |
| Iran | 1.7 | 2.8 | 3.1 | 3.5 | 4.3 |
| Iceland | 0.5 | 0.6 | 0.9 | 0.9 | 1.0 |

(*continued on next page*)

**Table 3** (*continued*)

| Country | Minimum | 1st Quartile | Median | 3rd Quartile | Maximum |
|---|---|---|---|---|---|
| Israel | 2.5 | 2.6 | 3.1 | 4.0 | 4.3 |
| Italy | 1.5 | 1.9 | 2.1 | 2.2 | 2.5 |
| Jamaica | 2.8 | 2.8 | 2.8 | 2.9 | 2.9 |
| Jersey | 0.9 | 0.9 | 0.9 | 0.9 | 0.9 |
| Jordan | 2.8 | 3.6 | 3.9 | 3.9 | 4.2 |
| Japan | 1.1 | 1.3 | 1.5 | 1.6 | 2.0 |
| Kazakhstan | 1.4 | 1.8 | 1.9 | 2.2 | 2.7 |
| Kenya | 2.2 | 2.5 | 2.7 | 2.9 | 4.9 |
| Kyrgyzstan | 2.1 | 2.3 | 2.5 | 2.6 | 2.8 |
| Kiribati | 2.6 | 2.6 | 2.6 | 2.6 | 2.6 |
| Korea, South | 1.5 | 1.7 | 1.8 | 1.9 | 2.1 |
| Kuwait | 2.6 | 2.6 | 2.6 | 2.6 | 2.6 |
| Lebanon | 2.4 | 2.4 | 2.4 | 2.4 | 2.4 |
| Libya | 3.0 | 3.1 | 3.4 | 4.1 | 4.7 |
| Lithuania | 0.9 | 1.3 | 1.3 | 1.4 | 1.4 |
| Luxembourg | 1.2 | 1.2 | 1.2 | 1.2 | 1.2 |
| Latvia | 1.1 | 1.2 | 1.3 | 1.3 | 1.4 |
| Macao | 1.0 | 1.0 | 1.0 | 1.0 | 1.0 |
| Morocco | 2.1 | 2.4 | 2.7 | 3.0 | 3.8 |
| Moldova | 1.6 | 1.6 | 1.6 | 1.6 | 1.6 |
| Madagascar | 2.2 | 2.3 | 2.5 | 2.8 | 3.1 |
| Mexico | 1.9 | 2.5 | 2.7 | 3.0 | 3.5 |
| Marshall Islands | 1.6 | 1.6 | 1.6 | 1.6 | 1.6 |
| North Macedonia | 2.1 | 2.1 | 2.2 | 2.2 | 2.2 |
| Mali | 2.3 | 2.8 | 3.3 | 3.5 | 3.7 |
| Malta | 2.3 | 2.3 | 2.3 | 2.3 | 2.3 |
| Myanmar | 1.9 | 1.9 | 1.9 | 1.9 | 1.9 |
| Montenegro | 2.1 | 2.1 | 2.1 | 2.2 | 2.2 |
| Mongolia | 1.8 | 2.1 | 2.2 | 2.4 | 2.6 |
| Northern Mariana Islands | 1.7 | 1.8 | 1.8 | 1.8 | 1.9 |
| Mozambique | 2.6 | 2.6 | 2.6 | 2.6 | 2.6 |
| Mauritania | 3.7 | 3.7 | 3.8 | 3.8 | 3.8 |
| Martinique | 2.8 | 2.8 | 2.8 | 2.8 | 2.8 |
| Mauritius | 1.7 | 1.9 | 2.2 | 2.5 | 2.6 |
| Malaysia | 1.8 | 2.1 | 2.1 | 2.2 | 2.6 |
| Mayotte | 2.7 | 2.7 | 2.7 | 2.7 | 2.7 |
| Namibia | 3.0 | 3.3 | 3.4 | 3.5 | 3.8 |
| New Caledonia | 2.1 | 2.1 | 2.2 | 2.5 | 2.8 |
| Niger | 2.3 | 2.6 | 2.7 | 2.9 | 3.7 |
| Norfolk Island | 1.8 | 1.8 | 1.8 | 1.8 | 1.8 |
| Netherlands | 0.8 | 0.9 | 0.9 | 1.0 | 1.1 |
| Norway | 0.5 | 0.7 | 0.8 | 1.0 | 1.6 |
| New Zealand | 0.8 | 1.0 | 1.1 | 1.2 | 1.3 |
| Oman | 2.8 | 3.4 | 3.6 | 3.9 | 4.8 |
| Pakistan | 2.7 | 2.8 | 3.0 | 3.1 | 3.2 |
| Peru | 1.8 | 2.3 | 2.8 | 3.1 | 3.5 |
| Philippines | 1.4 | 1.7 | 1.8 | 2.2 | 2.8 |
| Palau | 1.6 | 1.6 | 1.6 | 1.6 | 1.6 |
| Poland | 0.9 | 1.1 | 1.2 | 1.5 | 1.9 |
| Puerto Rico | 2.1 | 2.1 | 2.2 | 2.2 | 2.5 |
| Korea, North | 1.0 | 1.2 | 1.3 | 2.0 | 2.3 |
| Portugal | 1.0 | 1.8 | 2.0 | 2.2 | 2.6 |
| Paraguay | 2.1 | 2.3 | 2.3 | 2.4 | 2.7 |
| French Polynesia | 1.3 | 1.8 | 2.2 | 2.6 | 2.9 |
| Qatar | 2.5 | 2.5 | 2.5 | 2.5 | 2.5 |
| Reunion | 2.7 | 2.7 | 2.7 | 2.7 | 2.7 |
| Romania | 1.4 | 1.6 | 1.7 | 1.8 | 2.2 |
| Russia | 0.6 | 1.2 | 1.4 | 1.6 | 2.4 |
| Saudi Arabia | 2.6 | 4.1 | 4.3 | 4.4 | 4.9 |
| Senegal | 2.7 | 2.8 | 3.2 | 3.2 | 4.0 |
| Singapore | 2.0 | 2.0 | 2.0 | 2.0 | 2.0 |
| Saint Helena | 2.5 | 2.5 | 2.5 | 2.5 | 2.5 |
| Svalbard and Jan Mayen | 0.7 | 0.7 | 0.7 | 0.8 | 0.8 |
| Solomon Islands | 2.4 | 2.4 | 2.4 | 2.4 | 2.4 |
| Saint Pierre and Miquelon | 1.4 | 1.4 | 1.4 | 1.4 | 1.4 |
| Serbia | 1.4 | 1.7 | 1.8 | 1.9 | 2.2 |
| Slovakia | 1.5 | 1.7 | 1.7 | 1.8 | 2.5 |
| Slovenia | 1.6 | 1.6 | 1.6 | 1.7 | 1.8 |
| Sweden | 0.9 | 1.0 | 1.1 | 1.3 | 1.5 |

(*continued on next page*)

**Table 3** (*continued*)

| Country | Minimum | 1st Quartile | Median | 3rd Quartile | Maximum |
|---|---|---|---|---|---|
| Seychelles | 2.1 | 2.1 | 2.1 | 2.1 | 2.1 |
| Syria | 2.3 | 2.7 | 2.9 | 3.6 | 4.0 |
| Chad | 3.6 | 3.6 | 3.6 | 3.6 | 3.6 |
| Togo | 1.9 | 1.9 | 1.9 | 1.9 | 1.9 |
| Thailand | 1.7 | 1.9 | 2.4 | 2.6 | 2.7 |
| Tajikistan | 3.0 | 3.0 | 3.0 | 3.0 | 3.0 |
| Turkmenistan | 2.5 | 2.7 | 3.0 | 3.1 | 3.2 |
| Tonga | 1.6 | 1.8 | 1.9 | 2.0 | 2.2 |
| Trinidad and Tobago | 2.0 | 2.0 | 2.0 | 2.0 | 2.0 |
| Tunisia | 2.3 | 2.4 | 3.0 | 3.2 | 3.6 |
| Turkey | 1.3 | 2.2 | 2.5 | 2.6 | 2.9 |
| Taiwan | 0.8 | 1.3 | 1.5 | 1.8 | 2.3 |
| Tanzania | 2.5 | 2.5 | 2.5 | 2.5 | 2.5 |
| Ukraine | 1.3 | 1.5 | 1.6 | 1.7 | 1.9 |
| Uruguay | 1.8 | 1.9 | 2.0 | 2.1 | 2.2 |
| Uzbekistan | 2.2 | 2.4 | 2.8 | 2.9 | 3.1 |
| Venezuela | 1.7 | 1.9 | 2.1 | 2.1 | 2.1 |
| Viet Nam | 0.7 | 1.0 | 1.4 | 1.6 | 2.6 |
| Vanuatu | 1.9 | 2.0 | 2.1 | 2.2 | 2.2 |
| Wallis and Futuna | 2.0 | 2.0 | 2.0 | 2.0 | 2.0 |
| South Africa | 0.8 | 2.0 | 2.5 | 3.2 | 4.1 |
| Zimbabwe | 2.3 | 2.4 | 2.6 | 2.8 | 3.3 |
| United States | 0.4 | 1.8 | 2.1 | 2.6 | 4.3 |
| Canada | 0.6 | 1.1 | 1.4 | 1.5 | 2.5 |
| All Countries | 0.4 | 1.4 | 1.8 | 2.4 | 5.3 |

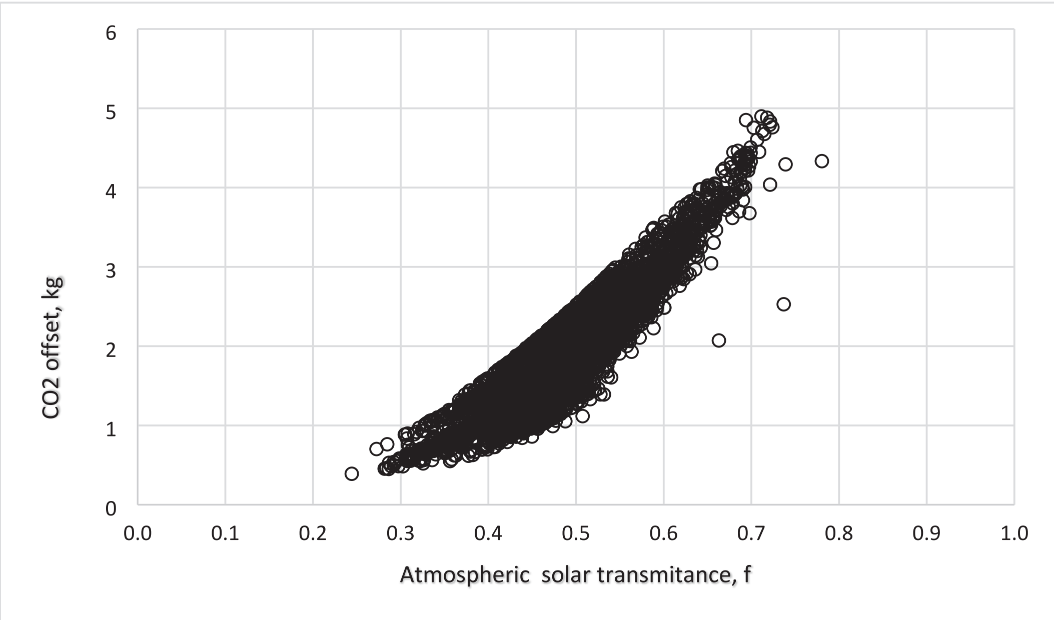


**Fig. 4.** $CO_2$ offset as a function of atmospheric solar transmittance.

2. For a given location (latitude $\varphi$), we then a) looked up for the $I_{TOA}$ using Fig. 1a; b) calculated the annual average atmospheric solar transmission, $f_{avg}$, by dividing the annual GHI from local weather stations by $I_{TOA}$; c) calculated the $CO_2$ offset (Eq. 13).

## 4. Results and discussions

Fig. 2 shows the measured GHI for all weather stations (data contains some apparent outliers). In extreme cases of very high and low latitudes, GHI is about 75 $Wm^{-2}$ (about 40% of the extraterrestrial solar radiation of a horizontal surface). For latitudes $-10^\circ$ to $10^\circ$, GHI is about 200 $Wm^{-2}$ (close to 48%) of $I_{TOA}$. For latitudes $-30^\circ$ to $-20^\circ$ and $20^\circ$ to $30^\circ$, GHI is the highest and approaches about 250 $Wm^{-2}$ (about 70% of $I_{TOA}$).

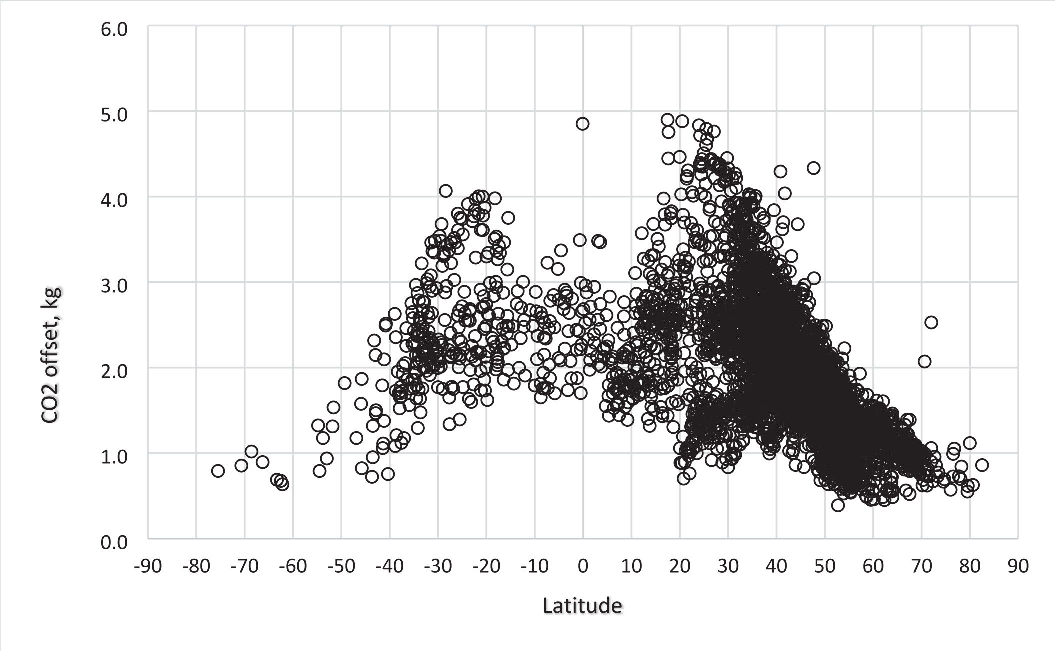


**Fig. 5.** Variation of $CO_2$ offset with latitude.

The fraction of solar energy transmitted through the atmosphere, $f$ is shown in Fig. 3 and summarized in Table 1. The median annual atmospheric transmittance is about 49%. The maximum transmittance is about 79% for the Northern Hemisphere (desert land in northern Africa and Middle East) and for the Southern Hemisphere 69% in Kenya and 67% in South Africa.

Kiehl and Trenberth (1997) estimate that of the total global average of 342 $Wm^{-2}$ incident shortwave solar radiation, 198 W $m^{-2}$ ($f = 0.58$) is transmitted through the atmosphere and reaches the earth's surface. NASA's estimate of atmospheric solar transmittance is 0.55 (see Table 2). These estimates include both land and ocean surfaces. The amount of cloud cover on ocean surfaces is typically higher than land surfaces (King et al., 2013). Hence, in Kiel and Trenberth calculations, the fraction of atmospheric transmittance over the land should be even higher than 0.55 or 0.58. This contrasts our calculated atmospheric solar transmittance of a median $f = 0.485$ for all weather stations around the world.

Using Eq. 13, we calculated the $CO_2$ offset for all weather stations. The results were then grouped and presented by countries and summarized by minimum, 25% quartile, median, 75% quartile, and maximum (see Table 3). The world-wide median $CO_2$ offset is about 1.8 kg. Akbari et al. (2009) estimate, based on Kiehl and Trenberth (1997) earth energy balance data, is 2.55 kg. The difference can almost entirely be explained by normalizing for the atmospheric transmittance of this study (0.485) and Kiehl and Trenberth (1997).

The variation of $CO_2$ offset with atmospheric transmittance is shown in Fig. 4. The $CO_2$ offset is highest where the atmospheric transmittance is greatest. As shown in Fig. 3., atmospheric transmittance is highest around latitude 20° to 30° and − 30° to −20°. The $CO_2$ offset is about 2–3 kg around the equator, 1.5–4 kg for −30° to −20° latitude and 1–5 kg for 20° - 30° latitude (see Fig. 5).

Table 3 $CO_2$ offset calculations are based on assumptions and simplifications used in Eq. 13. The constant is Eq. 13 is a linear function of current atmospheric $CO_2$ concentration. It is expected that the atmospheric $CO_2$ concentration to increase for at least the next few decades.

The fraction of emitted $CO_2$ that stays in the atmosphere used in our calculations is 0.50. Various studies show estimates of 0.45 to 0.55. This variation can introduce a ± 10% variance in our estimated $CO_2$ offset.

The incoming GHI reported in the typical weather years is estimated to be accurate within ±2–3%.

The seasonal $CO_2$ equivalency is a strong function of the incoming global solar radiation which in turn is a function of time of the year and regional cloud cover. To illustrate these variations, we performed monthly calculations for five locations: Abu Dhabi UAE, Sydney Australia, Montreal Canada, Aeroparque Argentina, and Phoenix AZ (see Fig. 6). Although the monthly GHI changed by up to a factor of four throughout the year, the monthly atmospheric transmittance only varied by up to 15%, for a given location. Also, the monthly variation in $CO_2$ equivalency was about a factor 2–3. The weighted average of the monthly $CO_2$ equivalencies for these four stations differed less than 0.5% than those of the annual calculations.

## 5. $CO_2$ offset based on RF and rise in global atmospheric temperature

The calculations of $CO_2$ offset based on the RF provide a current equivalency between $CO_2$ emissions and surface albedo modifications. Because of the Earth's inertia, the atmospheric temperature lags the RF changes by decades. Akbari et al. (2012) used the

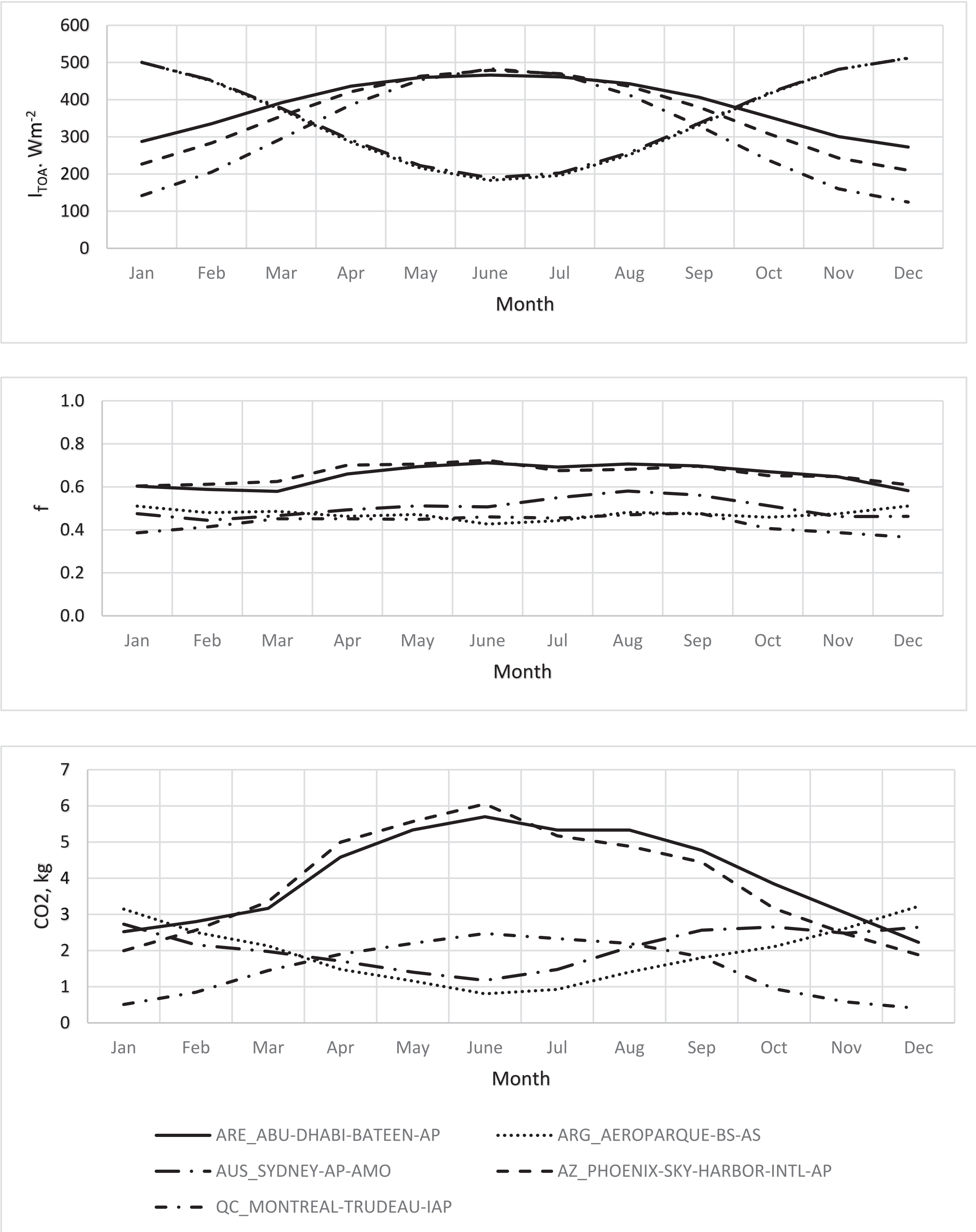


**Fig. 6.** a) The incoming top-of -the atmosphere solar intensity $I_{TOA,}$ b) Monthly averaged atmospheric solar transmittance $f_{monthly\ avg}$, c) monthly averaged $CO_2$ offset for five selected locations.

simulations of Matthews et al. (2012) that estimated that each 3700 Gt of emitted $CO_2$ results in a best guess of 1.75 K of global temperature change. Using this relationship, then the estimated $CO_2$ offset of increasing albedo of 1 $m^2$ of surface calculated at about 7 kg. On the other hand, Valone (2021) provides a simple correlation that each 20 ppm increase in atmospheric $CO_2$ concentration results in 1 K temperature rise of the globe. Based on this correlation and the correlation from Akbari et al. (2012) that changing surface albedo by 0.01 of a $m^2$ of surface results in $3.2 \times 10^{-15}$ K global temperature change, we estimate a $CO_2$ offset of 1 kg. Literature is saturated with models that estimate the temperature rise with increasing $CO_2$ emissions. Our $CO_2$ offset estimate of world average 2 kg for increasing albedo of a $m^2$ of surface by 0.01 falls within in the range of 1–7 kg from the two studies mentioned above.

## 6. Conclusions

We introduced a simplified technique to calculate a $CO_2$-equivalency (offset) for changes in the albedo of land surfaces areas on top of the atmosphere RF. Calculations were carried out for about 4400 weather stations world wide. The calculated world-wide median $CO_2$ offset was about 2 kg per 0.01 albedo change of a $m^2$ of a surface. The $CO_2$ offset is highest where the atmospheric transmittance is high, around latitude 20° to 30° and − 30° to −20°. The $CO_2$ offset is about 2–3 kg around the equator, 1.5–4 kg for −30° to −20° latitude and 1–5 kg for 20° to 30° latitude. This simplified method allows countries to develop policies monetizing the effect of high-albedo urban surfaces to counter global warming.

## CRediT authorship contribution statement

**Hashem Akbari:** Writing – review & editing, Writing – original draft, Visualization, Validation, Software, Methodology, Investigation, Funding acquisition, Formal analysis, Data curation, Conceptualization.

## Author's statement

Urban surfaces (roofs and pavements) with high solar reflectance absorb less of incoming shortwave solar radiation and stay cooler under the sun. A cool roof conducts less heat into the building resulting in less air-conditioning energy use in conditioned buildings and improved comfort in non-conditioned buildings. Cool roofs and cool pavements (together an independently) alter the surface heat balance at a community which can result in a lower summer time ambient temperature and reduced urban heat island. Lower summertime ambient temperatures typically result in a better ambient air quality (lower concentration of pollutants), improved pedestrian comfort, and lower morbidity and mortality during heat storms.

Cool roofs and pavements also reflect a significant fraction of incoming shortwave solar radiation that escape the Earth's atmosphere helping to counter global warming. This aspect of reflective surfaces is referred to as a geoengineering technology. Reducing atmospheric $CO_2$ concentration and increasing earth's albedo both cause a negative radiative forcing (RF) that result in slowing the rate of global warming. By equating the RF of incremental $CO_2$ emissions and increasing surface albedo, The Intergovernmental Panel for Climate Change (IPCC) in its 5th assessment report adopted this 7 kg $CO_2$ offset for increasing surface albedo (IPCC, 2014). Both studies reported only the world-wide effects; regional effects were not evaluated.

The RF from increasing surface albedo is expected to be most effective in regions with high insolation and less clouds. Here, we develop a method to calculate the incoming solar radiation on top of the atmosphere (TOA) for a given location. Then using locally available global horizontal insolation (GHI), we calculate the local atmospheric transmittance and top of the atmosphere RF by increasing a surface albedo. We equate this RF of albedo change with RF from $CO_2$ emissions to develop a *regional* equivalency between surface albedo change and $CO_2$ emission reduction. We carry out calculations for about 4400 stations around the world. The results are grouped together and presented by countries. The method can be used to develop a $CO_2$ equivalency (offset) and surface albedo change for a given location.

## Declaration of competing interest

I declare that this research is original and all the analyses are original and perform by myself. I further declare that I do no have any financial or other conflicts of interest in authoring this paper.

An earlier draft of this paper with limited results was presented at the 6th International Conference on Countermeasures to Urban Heat Island, Melbourne, Australia, December 4–7, 2023. This paper has modified the methodology and provides detail results for over 200 countries.

## Acknowledgement

Funding for this research was provided by the Natural Sciences and Engineering Research Council of Canada under the discovery program. This research was in part funded by: Juan Carlos Pereira, President of Instituto Provincial de Desarrollo Habitacional (IPRODHA) - (Provincial Institute of Housing Development), Gervasio Malagrida, Minister of Climate Change, Province of Misiones Argentina, and MACOMA Environmental Technologies, Corp. Nevada, USA.

## Data availability

Data will be made available on request.

## References

Akbari, H., Konopacki, S., Pomerantz, M., 1999. Cooling energy savings potential of reflective roofs for residential and commercial buildings in the United States. Energy 24, 391–407.
Akbari, H., Menon, S., Rosenfeld, A., 2009. Global cooling: increasing world-wide urban albedos to offset $CO_2$. Clim. Chang. 95 (3–4).
Akbari, H., Matthews, H.D., Seto, D., 2012. The long-term effect of increasing the albedo of urban areas. Environ. Res. Lett. 7, 024004 (10pp).
ASHRAE, 2012. International Weather for Energy Calculations Version 2" (IWEC2), American Society of Heating, Refrigerating, and Air-Conditioning Engineers, Atlanta GA. Technical Report: Huang, Y.J. 2011. "ASHRAE Research Project 1477-RP (Development of 3,012 Typical Year Weather Files for International Locations). Final Report, ASHRAE, Atlanta Ga.
"Frequently Asked Questions". Carbon dioxide information analysis Center (CDIAC). Archived from the original on *17 August* 2011. *(*Retrieved 13 June 2007).
George, K., Ziska, L.H., Bunce, J.A., Quebedeaux, B., 2007. Elevated atmospheric CO2 concentration and temperature across an urban–rural transect. Atmos. Environ. 41 (35), 7654–7665. Bibcode:2007AtmEn..41.7654G. https://doi.org/10.1016/j.atmosenv.2007.08.018. Archived from the original on 15 October 2019. Retrieved 12 September 2019.
Hosseini, M., Akbari, H., 2016. Effect of cool roofs on commercial buildings energy use in cold climates. Energ. Buildings **114**, 143–155.
IPCC, 2014. In: Lucon, O., Ürge-Vorsatz, D., Ahmed, A. Zain, Akbari, H., et al. (Eds.), Chap 9. Cambridge University Press, Cambridge, United Kingdom and New York, NY, USA, p. 699.
Jandaghian, Z., Akbari, H., 2021. Increasing urban albedo to reduce heat-related mortality in Toronto and Montreal, Canada. Energ. Buildings 237.
Kiehl, J.T., Trenberth, K.E., 1997. Earth's annual global mean energy budget. Bull. Am. Meteorol. Soc. 78 (2), 197–208. February.
King, D.M., Platnick, S., Menzel, W.P., Ackerman, S.A., Hubanks, P.A., 2013. Spatial and Temporal Distribution of Clouds Observed by MODIS Onboard the Terra and Aqua Satellites. IEEE Trans. Geosci. Remote Sens. 51 (7). July.
Loeb, Norman G., Johnson, Gregory C., Thorsen, Tyler J., Lyman, John M., et al., 2021. Satellite and ocean data reveal marked increase in earth's heating rate. Geophys. Res. Lett. 48 (13), 15 June.
Merket, Noel, 2020. Weather data for buildings energy simulations. In: NREL Data Catalog. Golden, CO: National Renewable Energy Laboratory. Last updated: July 24, 2024. https://doi.org/10.7799/1603006.
Myhre, G., Highwood, E.J., Shine, K.P., Stordal, F., 1998. New estimates of radiative forcing due to well mixed greenhouse gases. Geophys. Res. Lett. 25 (14), 2715–2718. July 15.
NOAA, 2022. Carbon dioxide now more than 50% higher than pre-industrial levels. National Oceanic and Atmospheric Administration. *www.noaa.gov*. Retrieved 14 June.
NREL, 2008. TMY3 data for 1,020 US locations, technical report. In: Wilcox, S., Marion, W. (Eds.), User's Manual for TMY3 Data Sets, NREL/TP-581-43156. National Renewable Energy Laboratory, Golden CO.
Rasmussen, Carl Edward, . Atmospheric Carbon Dioxide Growth Rate. *Archived from the original on 14 March 2023. Retrieved 14 March*.
Valone, T.F., 2021. Linear Global Temperature Correlation to Carbon Dioxide Level, Sea Level, and Innovative Solutions to a Projected 6°C Warming by 2100. J. Geosci. Environ. Protect. 9, 84–135.
Vaughan, N.E., Lenton, T.M., 2011. A review of climate geoengineering proposals. Clim. Chang. 109, 745–790.
White Box Technologies, 2014. CN2014 Typical Year Weather Data for 226 Canadian Locations, Moraga CA (no technical report).
Wikipedia and its relevant references. Retrieved 8 December 2025.